AIAA 81-0646R

Improved Potential Gradient Method to Calculate Airloads on Oscillating Supersonic Interfering Surfaces

M. H. L. Hounjet*
National Aerospace Laboratory, NLR, Amsterdam, the Netherlands

A description is given of a computationally improved potential gradient method to calculate unsteady aerodynamic derivatives in supersonic flow. Results are presented and comparisons are made with results of existing methods and with experimental data for a fighter-type wing.

Nomenclature

B = $\sqrt{M^2-1}$
c = chord
C = matrix of influence coefficients
C_p = pressure coefficient, nondimensionalized with q
C_{zi} = sectional normal force coefficient in AGARD notation, Eq. (7)
C_{mi} = sectional pitching moment about quarter-chord point coefficient in AGARD notation, Eq. (8), C^*_{mi} is moment about midchord
F = variation of the potential jump behind the leading edge of an element on which a constant potential gradient in streamwise direction is assumed (Fig. 1b)
h = amplitude of the normal displacement of the oscillating wing
k = reduced frequency = $\omega l/U$
K = supersonic pressure dipole kernel
l = reference length
M = Mach number
n = normal directions of receiving wings
N = total number of unknowns
q = dynamic pressure = $\frac{1}{2}\rho U^2$
Q_{mn} = generalized aerodynamic coefficients, generalized forces, Eq. (6)
r = $\sqrt{y^2+z^2}$
r_h = $\sqrt{x^2-B^2(y^2+z^2)}$
S = surface
s = semispan
U = freestream velocity
u, v = orthogonal coordinates
W = modified upwash
x,y,z = orthogonal coordinates (nondimensionalized with l)
γ = $-kM^2/B^2$
γ_s, γ_r = dihedral angles of sending and receiving wings
λ = kM/B^2
ρ = density
φ = disturbance velocity potential
ϕ = modified disturbance velocity potential = $\varphi e^{-i\gamma x}$
ω = angular frequency
∇ = area of integration formed by the domain of dependence of the receiving point and the sending surface

Subscripts

k = kth streamwise strip
l = lth element
LE, le = leading edge of wing strip, element (Fig. 1)
TE, te = trailing edge of wing strip, element (Fig. 1)

Superscripts

i = ith streamwise strip
j = jth element
Δ = jump operator across the wing or wake surface, $\Delta A = A(x,y,0+) - A(x,y,0-)$
Δy = width of strip
Δx = length of element
ΔC_p = $C_p(x,y,0-) - C_p(x,y,0+)$

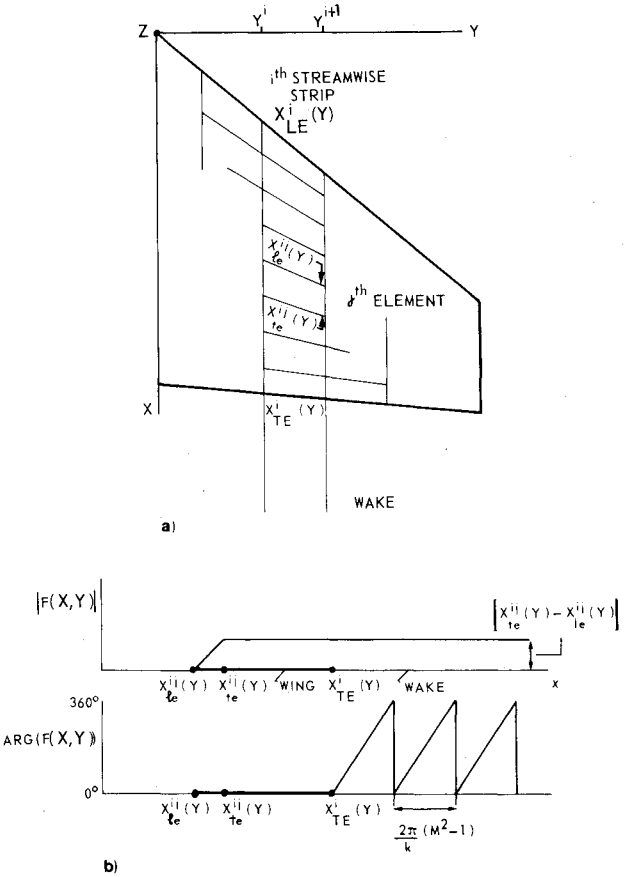

Fig. 1 The boundary element method.

Presented as Paper 81-0646 at the AIAA Dynamics Specialists Conference, Atlanta, Ga., April 9-10, 1981; submitted April 24, 1981; revision received Oct. 6, 1981.

*Research Engineer, Department of Aeroelasticity.

I. Introduction

AT NLR a comparative study was made a couple of years ago of methods to calculate unsteady airloads on oscillating interfering surfaces in supersonic flow. The method to be selected for programming should accomplish the following tasks: 1) deliver unsteady airloads for flutter clearance calculations for military aircraft, and 2) support wind-tunnel measurements of unsteady pressure distributions on oscillating wings.

Several methods were considered, based on different elementary solutions of the basic differential equation (source, velocity dipole, and pressure dipole) and on different solution techniques (collocation methods and boundary element methods). In spite of the considerable number of methods being proposed in the course of years, only the potential gradient method of Jones and Appa[1] remained as a candidate that would be able to answer satisfactorily the purposes mentioned above.

During the development of the present potential gradient method it turned out that the original integration procedure of Ref. 1 with respect to the wake and the far field elements could be improved substantially. The present paper describes this improvement and presents results of comparisons with other calculation methods and with experimental data for a fighter-type wing.

II. Aerodynamic Analysis

The boundary value problem governing the linearized unsteady flowfield induced by harmonically oscillating thin wings in supersonic flow is well known.[2] The basic differential equation for the disturbance velocity potential φ and the boundary conditions have been expressed by Jones[3] in terms of the more convenient modified potential ϕ:

$$\varphi = \phi e^{i\gamma x} \tag{1}$$

where

$$\gamma = -kM^2/B^2 \tag{2}$$

and

$$B^2 = M^2 - 1 \tag{3}$$

The boundary value problem can then be expressed by the integral equation

$$(h_x + ikh)e^{-i\gamma x} = -\left[\left(\cos(\gamma_r - \gamma_s)\frac{\partial}{\partial z} - \sin(\gamma_r - \gamma_s)\frac{\partial}{\partial y}\right)\frac{\partial}{\partial z}\right.$$

$$\left.\times \int\int_{\nabla_{\text{wing}} + \nabla_{\text{wake}}} \Delta\phi(u,v)\cos\lambda r_h/(2\pi r_h)\,du\,dv\right] \tag{4}$$

the Kutta condition and the additional relation in the wake is expressed by

$$\Delta\phi(x,y) = \Delta\phi[x_{\text{TE}}(y),y]e^{i[x-x_{\text{TE}}(y)]\lambda/M} \qquad x \geq x_{\text{TE}}(y) \tag{5}$$

where $\lambda = -\gamma/M$, $r^2 = y^2 + z^2$, and $r_h^2 = x^2 - B^2r^2$. $\nabla_{\text{wing}} + \nabla_{\text{wake}}$ denotes the domain of influence of wing and wake bounded by the intersection of the forward Mach cone with vertex at (x,y,z). The Cartesian coordinate system (x,y,z) is chosen fixed to the mean position of the sending wing with the x axis pointing in streamwise direction and the z axis normal to the sending wing mean surface. φ is the disturbance velocity potential. γ_r and γ_s denote the dihedral angle of the receiving and sending wing mean surfaces and h denotes the amplitude of the oscillation normal to the receiving wing mean surface.

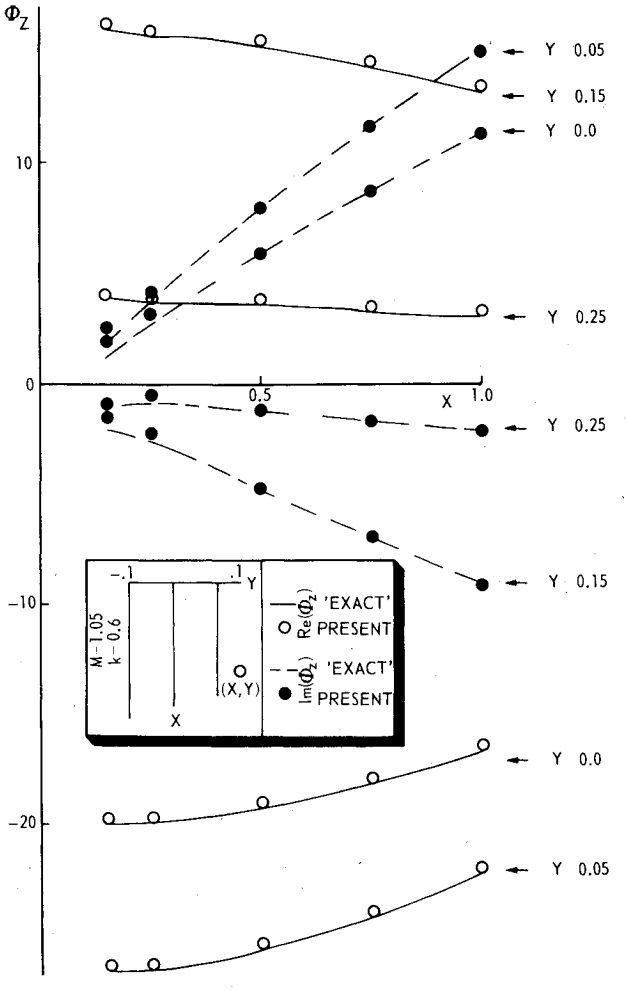

Fig. 2 The upwash due to the wake.

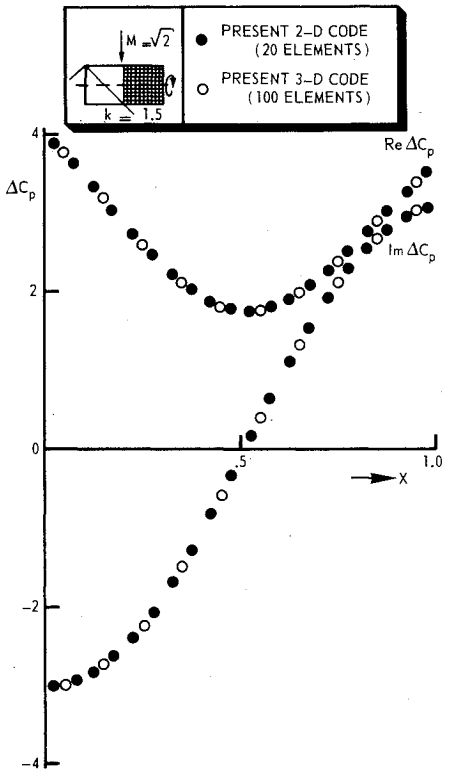

Fig. 3 Unsteady pressure distribution in midsection of rectangular wing ($\mathcal{A}R = 2$).

M is the freestream Mach number and k is the reduced frequency, $k=\omega l/U$. $x_{TE}(y)$ denotes the position of the trailing edge of the sending wing. The aforementioned variables are all made dimensionless with the reference length l and the oncoming flow U. Equation (4) must be applied for any combination of receiving and sending wings.

III. Definition of Unsteady Airloads

Generalized aerodynamic coefficients (generalized forces) are obtained by integrating the pressure and the displacement modes:

$$Q_{mn}=\int_{S_{wing}}\int \Delta C_{p_n} h_m \mathrm{d}x\mathrm{d}y \tag{6}$$

where ΔC_{p_n} represents the pressure jump across the wing due to the displacement mode h_n. Q_{mn} is made dimensionless with ql^3. Sectional lift and pitching moment about the quarter-chord coefficients are obtained by integrating the pressure difference along the streamwise section and put into standard AGARD notation[4]:

$$C_{zi}(y)=\frac{1}{2\pi}\int_{-1}^{1}\Delta C_p \mathrm{d}\bar{x}=-\frac{1}{\pi}\Delta\varphi[x_{TE}(y)]-\frac{ik}{\pi}\int_{-1}^{1}\Delta\varphi \mathrm{d}\bar{x} \tag{7}$$

$$C_{mi}(y)=\frac{1}{2\pi}\int_{-1}^{1}\Delta C_p(\bar{x}-0.5)d\bar{x}=-\frac{3}{4\pi}\Delta\varphi[x_{TE}(y)]$$

$$+\frac{1}{\pi}\int_{-1}^{1}\Delta\varphi[1-ik(\bar{x}-0.5)]\mathrm{d}\bar{x} \tag{8}$$

where

$$\bar{x}=2\{x-[x_{TE}(y)+x_{LE}(y)]/2\}/[x_{TE}(y)-x_{LE}(y)]$$

$x_{LE}(y)$ denotes the position of the wing leading edge.

IV. Potential Gradient Method

To solve the integral Eq. (4) Jones and Appa[1] have adopted a boundary element method which employs a linear streamwise approximation of the potential jump on each element, in such a way that the approximation is continuous in streamwise direction at the element edges. The integration Eq. (4) can then be obtained in closed form without the need of distribution theory or "finite part" techniques. This section merely summarizes the potential gradient method of Ref. 1 to enable an explanation of what kind of improvements have been made for the development of the present method (see Sec. V).

The wing and wake are divided into streamwise strips and the wing part is subdivided into elements on which a constant modified potential gradient in streamwise direction is assumed (Fig. 1a). After requiring in one point of each element that the flow be compatible with the wing motion, an algebraic system results for the potential gradients:

$$W_{kl}=\sum_i\sum_j C^{ij}_{kl}\Delta\phi^{ij}_x \tag{9}$$

where W_{kl} represents the upwash on the lth element in the kth streamwise strip of the receiving wing and C^{ij}_{kl} represents the contribution to the upwash due to a constant modified potential gradient $\Delta\phi^{ij}_x$ on the jth element in the ith streamwise strip of the sending wing:

$$C^{ij}_{kl}=-\frac{1}{2\pi}\left[\cos(\gamma_r-\gamma_s)\frac{\partial}{\partial z}-\sin(\gamma_r-\gamma_s)\frac{\partial}{\partial y}\right]\frac{\partial}{\partial z}$$

$$\times\int\int_{\nabla^{ij}_{kl}} F^{ij}(u,v)(\cos\lambda r_h)/r_h \mathrm{d}u\mathrm{d}v \tag{10}$$

where ∇^{ij}_{kl} is the area of integration formed by the domain of dependence of the upwash point at the lth element in the kth streamwise strip of the receiving wing and the part of the strip behind the leading edge of the jth element in the ith streamwise strip of the sending wing. F^{ij} represents the modified dipole strength (potential jump) distribution in the ith streamwise strip generated by the constant modified potential gradient at the jth element in the ith streamwise strip. The functional variation of F is shown in Fig. 1b. The system Eq. (9) must be applied for any combination of receiving and sending wings.

Next, $\cos\lambda r_h/r_h$ is expanded in series form, after which closed form expressions to Eq. (10) can be obtained:

$$C^{ij}_{kl}=\sum_n A_{2n}W_{2n} \qquad n=0,1\ldots \tag{11}$$

where

$$W_{2n}=-\frac{1}{2\pi}\left[\cos(\gamma_r-\gamma_s)\frac{\partial}{\partial z}-\sin(\gamma_r-\gamma_s)\frac{\partial}{\partial z}\right]\frac{\partial}{\partial z}$$

$$\times\int\int_{\nabla^{ij}_{kl}} F^{ij}(u,v)r_h^{2n-1}\mathrm{d}u\mathrm{d}v \tag{12}$$

The W_{2n} are obtained in closed form[1] with respect to the integration over the wing part. Over the wake part the integration is performed by subdividing the strip into elements where F is approximated by constant potential gradients, after which the contribution of each element is obtained in closed form.

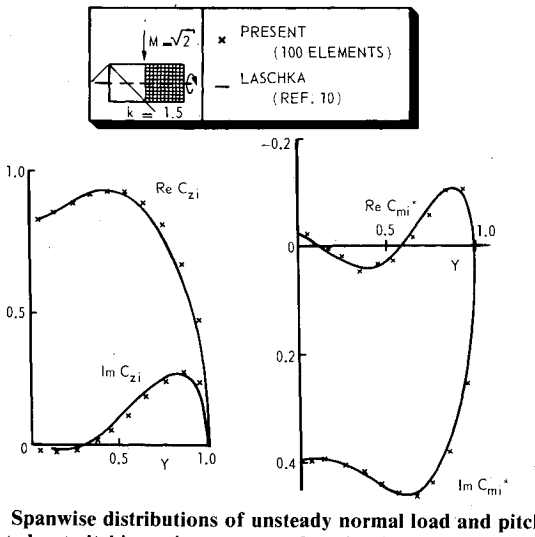

Fig. 4 Spanwise distributions of unsteady normal load and pitching moment about pitching axis on rectangular wing ($\mathcal{R}=2$).

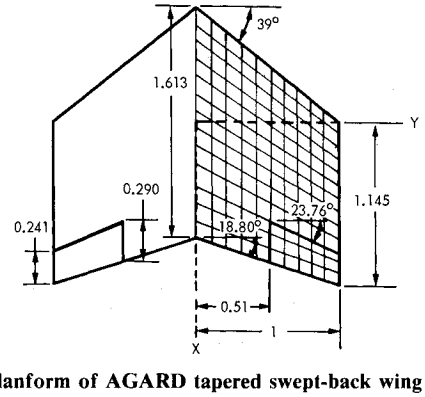

Fig. 5 Planform of AGARD tapered swept-back wing with control surface ($\mathcal{R}=1.45$).

Table 1 AGARD swept-back wing with control surface (Fig. 5) $\mathcal{R} = 1.45$. Modes[a]: 1) heaving; 2) pitching; 3) chordwise bending; 4) flapping of control surface. Mach 1.2

Methods (No. elements)	Q_{mn}	$k=0.5$ MOD(Q)	$k=0.5$ ARG(Q), deg	$k=1.0$ MOD(Q)	$k=1.0$ ARG(Q), deg	Q_{mn}	$k=0.5$ MOD(Q)	$k=0.5$ ARG(Q), deg	$k=1.0$ MOD(Q)	$k=1.0$ ARG(Q), deg
Present (150)		1.741	91.11	3.697	98.34		3.685	−8.75	2.892	4.75
Ref. 1 (147)		1.620	83.77	3.486	100.16		3.949	−7.44	2.644	−0.30
Ref. 11 (600)	1,1	1.675	90.78	3.570	96.50	1,3	3.406	−10.11	2.572	3.48
Ref. 12 (1734)		1.740	89.64	3.665	95.78		3.574	−9.74	2.720	3.69
Present		0.277	176.94	0.891	143.43		2.842	−9.54	2.333	5.39
Ref. 1		0.248	159.98	1.012	147.82		3.025	−12.09	2.008	2.36
Ref. 11	2,1	0.283	179.15	0.868	144.70	2,3	2.753	−11.00	2.213	2.58
Ref. 12		0.279	175.78	0.904	143.00		2.864	−10.81	2.301	2.94
Present		0.331	121.09	0.916	114.28		1.468	−4.56	1.378	20.02
Ref. 1		0.261	117.23	0.946	113.95		1.556	−6.25	1.218	24.88
Ref. 11	3,1	0.322	120.71	0.877	112.79	3,3	1.362	−5.24	1.270	20.09
Ref. 12		0.333	119.15	0.912	112.57		1.450	−5.07	1.346	19.85
Present		0.012	140.88	0.031	132.00		0.079	6.54	0.086	27.10
Ref. 1		0.010	158.52	0.036	120.88		0.067	−2.09	0.064	35.34
Ref. 11	4,1	0.012	140.95	0.032	134.36	4,3	0.081	7.03	0.089	27.72
Ref. 12		0.013	141.34	0.034	132.61		0.086	7.37	0.094	27.93
Present		3.923	14.12	4.575	24.04		0.556	−1.63	0.531	−1.97
Ref. 1		3.569	10.02	4.492	24.98		0.556	−0.88	0.531	−0.58
Ref. 11	1,2	3.772	13.28	4.370	21.24	1,4	0.572	−1.49	0.544	−1.77
Ref. 12		3.902	12.41	4.490	21.02		0.590	−1.99	0.561	−2.76
Present		1.266	78.05	1.966	65.78		0.498	−1.40	0.474	−1.35
Ref. 1		1.218	85.73	2.040	64.06		0.498	−0.60	0.475	0.12
Ref. 11	2,2	1.253	78.77	1.914	65.25	2,4	0.510	−1.24	0.483	−1.10
Ref. 12		1.278	77.02	1.983	64.37		0.532	−1.72	0.502	−2.05
Present		0.985	44.64	1.335	45.36		0.450	−1.16	0.427	−0.67
Ref. 1		0.859	45.17	1.291	41.53		0.449	−1.10	0.424	−0.80
Ref. 11	3,2	0.944	43.73	1.255	43.47	3,4	0.458	−0.93	0.433	−0.30
Ref. 12		0.979	42.99	1.313	43.52		0.483	−1.54	0.455	−1.51
Present		0.041	62.81	0.062	66.77		0.050	1.51	0.042	6.09
Ref. 1		0.040	71.07	0.055	56.34		0.045	2.68	0.042	7.88
Ref. 11	4,2	0.041	63.25	0.064	68.28	4,4	0.051	1.78	0.048	6.21
Ref. 12		0.044	62.85	0.066	66.92		0.053	1.08	0.049	−4.67

[a] Modes are defined in the text.

V. New Formulations in the Present Method

The original approach of Ref. 1, where closed form expressions to Eq. (10) were obtained by expanding $\cos\lambda r_h / r_h$ in series form, works well as long as 1) the contribution of the wake in the integration area in Eq. (12) remains small and 2) λ and r_h are not too large. These conditions are fulfilled in general for single wings.

For configurations with interfering surfaces, however, the evaluation of the integral in Eq. (12) becomes time-consuming because of the large wake part. For large λ and r_h numerical inaccuracy may arise, which can be removed by adding more terms in the expansion at the expense of increased computational labor. Also, Ref. 1 mentions the latter problem, and in the original method a distinction was made, therefore, between influences of near field elements and easier-to-compute influences of far field elements. The extent of the near field, however, may not be uniform for all configurations and flow parameters and probably may not even be small.

In the present method the above-mentioned objections have been relieved by applying a different integration procedure in Eq. (10) without an expansion as in Eqs. (11) and (12), which is used *whenever the whole sending wing part of a strip lies in the domain of dependence of the receiving point.* As the integrand has no singularities, the integration over the wing is straightforward and numerical integration is applied. The integration over the wake can be recognized to be a line integration of the supersonic pressure dipole kernel[5]† along the trailing edge of the strip. The kernel function is evaluated using the approximations presented in Ref. 6.‡ The line integration is performed with the same technique as used in the doublet lattice method[7]:

$$C_{kl}^{ij} = -\frac{1}{2\pi}\left[\cos(\gamma_r - \gamma_s)\frac{\partial}{\partial z} - \sin(\gamma_r - \gamma_s)\frac{\partial}{\partial y}\right] \times \frac{\partial}{\partial z}\sum_{m=j}^{j_{TE}(i)}\sum_{p=1}^{PG}\omega_m^p \Big\{F^{ij}(u,v) \times (\cos\lambda r_h / r_h)\Big\}_{u=x_m^p,\ v=y_m^p} + (C_{kl}^{ij})_{\text{wake}} \tag{13}$$

where

$$C_{kl_{\text{wake}}}^{ij} = \frac{e^{-ix\gamma y}}{2}\int_{y^i}^{i+1} I\,dv \tag{14}$$

†The pressure dipole kernel as presented in Ref. 5 is not complete for receiving points at the rearward Mach cone surface of the sending point.[6] In the present case the pressure dipole kernel is complete because the receiving points do not lie on that Mach cone surface.

‡The present technique is slightly different because one of the sets of coefficients used in Ref. 6 has been exchanged for a set developed in Ref. 8.

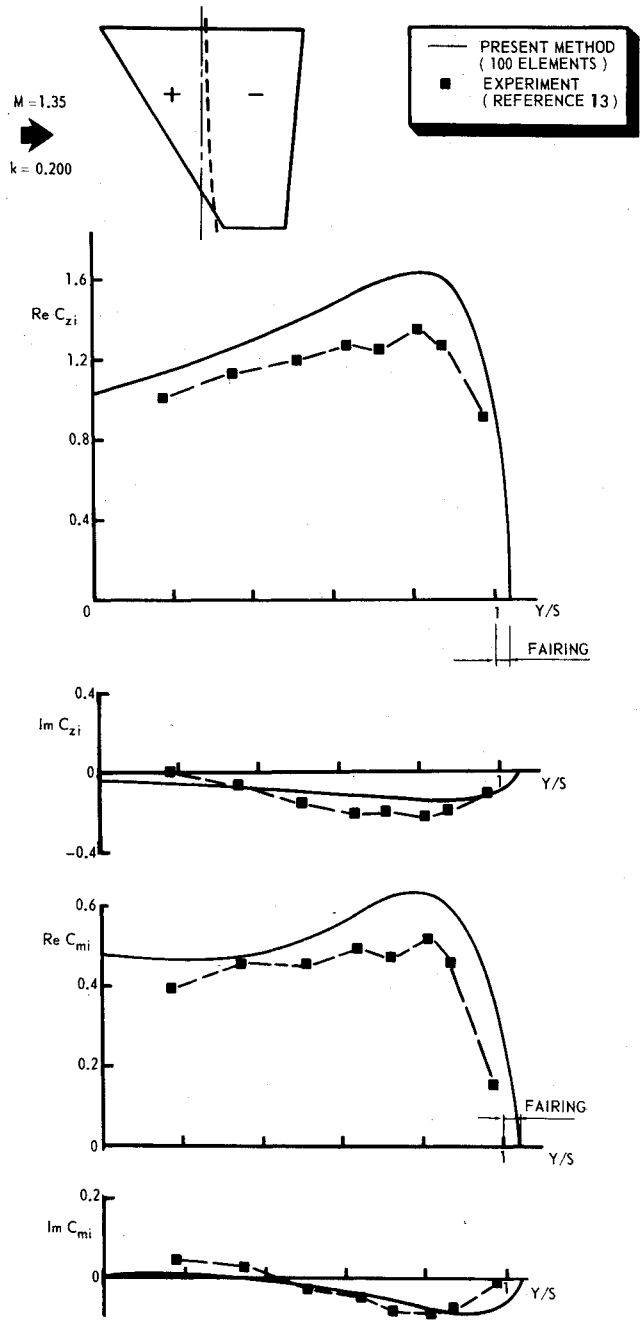

Fig. 6 Unsteady spanwise normal load and pitching moment distributions at $k=0.200$.

and

$$I=F^{ij}[x_{TE}(v),v]e^{i\gamma x_{TE}(v)}K[x-x_{TE}(v),$$
$$y-v,z;\gamma_r,\gamma_s,k,M] \tag{15}$$

m denotes the wing elements in the ith streamwise strip. The ω_m^p are Gaussian weight factors and x_m^p, y_m^p are abscissas at the mth wing element in the ith streamwise strip. $j_{TE}(i)$ indicates the last wing element in the ith streamwise strip. The required value of PG is chosen depending on r_h, λ, Δx, and Δy (e.g., $PG=1$ when $r_h>\Delta x$, Δy, and $\lambda<1/\Delta x$, $1/\Delta y$ suffice).

K represents the supersonic pressure dipole kernel[5] which is split up into a planar part K_1/r^2 and a nonplanar part K_2/r^4. Accordingly, I is expressed as

$$I=I_1/r^2+I_2/r^4 \tag{16}$$

The wake contribution is evaluated as

$$(C_{kl}^{ij})_{wake}\approx\frac{e^{-i\gamma x}}{2}\sum_{ii=1}^{NS}\int_{v_{ii}}^{v_{ii+1}}[\tilde{I}_1^{ii}/r^2+\tilde{I}_2^{ii}/r^4]\,dv \tag{17}$$

where the required value of NS is chosen depending on Δy and $r_{h_{TE}}=[[x-x_{TE}(v)]^2-B^2r^2]^{1/2}$ (e.g., $NS=1$ when $r_{h_{TE}}>\Delta y$ suffices). $\tilde{I}_{1,2}^{ii}$ are parabolic approximations to $I_{1,2}$ in interval ii:

$$\tilde{I}_{1,2}^{ii}=A_{1,2}^{ii}+B_{1,2}^{ii}v+C_{1,2}^{ii}v^2 \tag{18}$$

The coefficients A, B, and C are obtained by the determination of K_1 and K_2 at v_{ii}, $v_{ii+1/2}$, and v_{ii+1} with the numerical techniques of Ref. 6. The integrations in Eq. (17) are obtained in closed form.[7] No use is made of the possibility to subtract the steady part of the kernel and to deal with it analytically.

The feasibility of this method is demonstrated in Fig. 2, which shows $\phi_z=(C_{kl}^{ij})_{wake}$ for a trailing edge without sweep in the planar case for $M=1.05$, $k=0.6$, and $F[x_{TE}(y),y]=1$. The calculations have been made with the present approach and with the original method of Jones and Appa. This test case is considered to be severe because the value of λ is about 6. The results according to the original method converged to stable values by applying a very small step size. These results are indicated as "exact." The present results have been obtained by taken $NS=11$. The large number guarantees convergence of the results.

VI. Computational Aspects of the Present Method

This section describes briefly some aspects of the NLR computer program, such as the grid system, the choice of the location of the upwash points, the displacement modes, the matrix-solution method, and the computer cost.

Grid System

The type of the quadrilateral element with chordwise sides parallel to the x axis facilitates an automatic grid generation. The present method requires the input of a coarse idealization of the configuration into quadrilateral segments with chordwise sides parallel to the x axis or triangular segments with chordwise sides parallel to the x axis. These segments will be automatically divided into a required number of strips of quadrilateral elements with chordwise sides parallel to the x axis.

Upwash Points

The upwash points are also automatically generated. Experience with numerical experiments with two- and three-dimensional supersonic and subsonic potential gradient methods has shown that

1) if the leading edge of the element is supersonic the choice of 50% of the element chord as location of the upwash points gives satisfactory results;

2) in the case of a subsonic leading edge the choice has to be 85%;

3) if the trailing edge of the wing is subsonic the upwash points on the elements just before the trailing edge are chosen to lie at 92.5%. The Kutta condition which requires zero pressure jump at subsonic trailing edges is "satisfied" by this selection.

Displacement Modes

The displacement modes of the segments are also automatically generated in the elements. The user has control of three modes for each segment: 1) normal translation; 2) rotation about an arbitrary axis; and 3) control surface

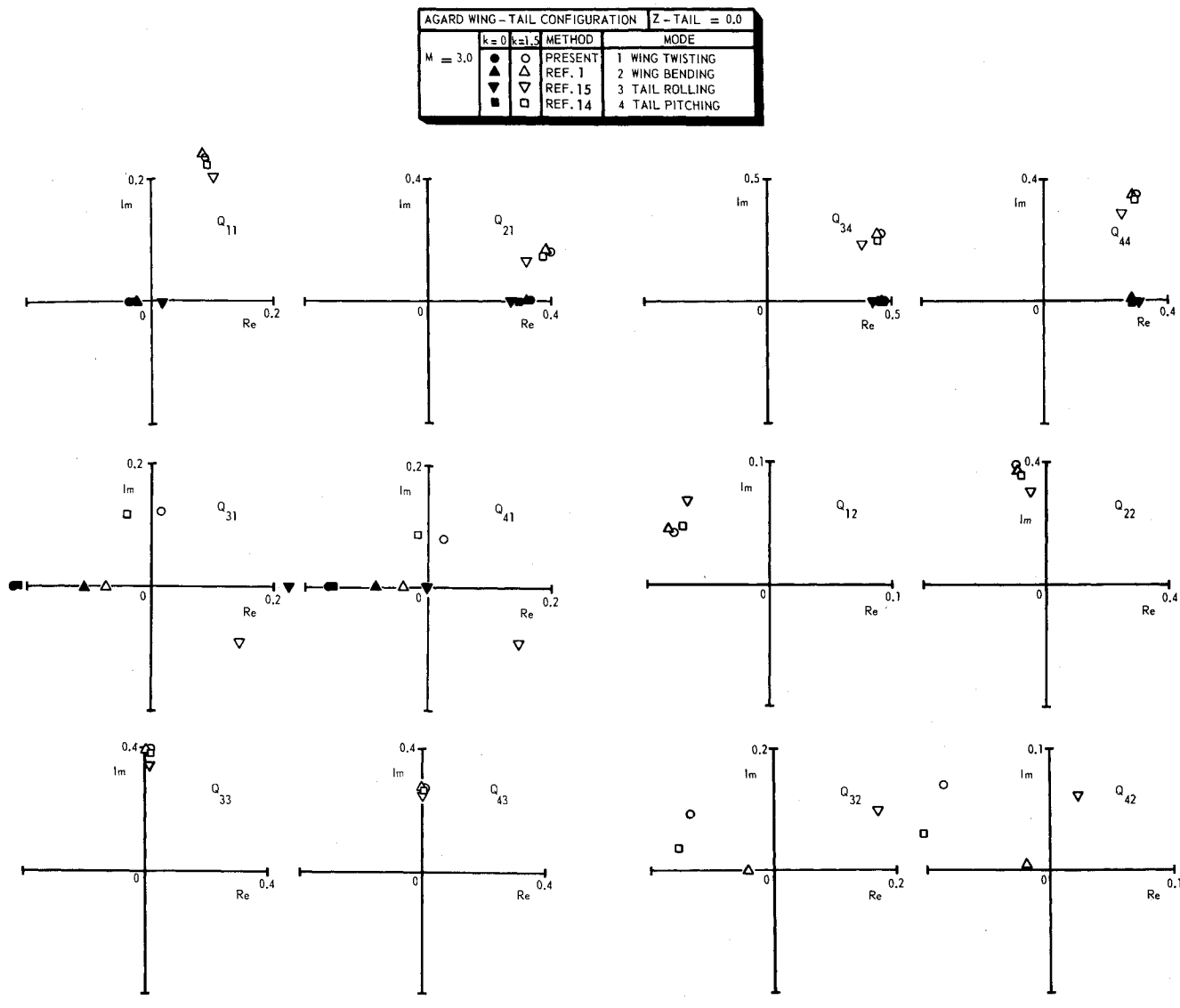

Fig. 7 Polar plots of generalized aerodynamic coefficients for AGARD wing-tail configuration.

rotation about the leading or trailing edge of the control surface. Each mode can be replaced by a zero displacement mode. Other modes require the input of polynomial coefficients for each segment.

Solution Method

The set of linear equations defined by Eq. (9) is solved by applying the Crout factorization method. This factorization has to be performed only once for all displacement modes. This procedure has the advantage of a low computer cost to find a solution for each displacement mode, although the computer cost to perform the Crout factorization is rather high (asymptotic operation count is $O(N^3)$, where N is the number of elements).

If iterative methods would be applied, the linear system has to be solved separately for each displacement mode, although the solution procedure itself is usually more economical. In the future possibly an iterative method may be incorporated in order to select the most economical method for a given set of calculations.

Computer Cost

The computer cost depends mainly on the CPU time that is necessary for the determination of the influence coefficients C_{kl}^{ij} and the CPU time that is needed to perform the Crout factorization. The CPU time needed to compute the influence coefficients, in turn, depends on Mach number, reduced frequency, and configuration. For a typical configuration such as the AGARD wing-tail configuration, which will be discussed in Sec. VII, this part is about $0.004N^2$ seconds for the CDC Cyber 72,§ where N is the number of elements.

The CPU time to perform the Crout factorization is about $0.00002\,N^3$ seconds.

Table 2 Displacement modes of AGARD wing-tail configuration

Wing	Tail	Mode
$h_1 = y(x - 2.25\,\lvert y\rvert - 0.85)$	0	Wing twisting
$h_2 = y\,\lvert y\rvert$	0	Wing bending
$h_3 = 0$	y	Tail rolling
$h_4 = 0$	$\text{sign}(y) \times (x - 3.35)$	Tail pitching

§CDC Cyber 72 is about three times slower than a CDC 6600.

Table 3 AGARD wing-tail interference, z tail = 0.6.
Modes[a]: 1) wing twisting; 2) wing bending; 3) tail rolling; 4) tail pitching

Mach no.	Methods (No. elements)	Q_{mn}	$k=0.0$ MOD(Q)	$k=0.0$ ARG(Q), deg	$k=1.5$ MOD(Q)	$k=1.5$ ARG(Q), deg
	Present (170)	1,1	0.0285	180.00	0.2512	68.57
	Ref. 14		0.0340	180.00	0.2375	67.40
	Present	2,1	0.3386	0.00	0.4335	21.60
	Ref. 14		0.3160	0.00	0.4029	19.35
	Present	3,1	0.1194	180.00	0.2086	63.57
	Ref. 14		0.1296	180.00	0.1504	33.55
	Present	4,1	0.0821	180.00	0.1495	68.69
	Ref. 14		0.0957	180.00	0.1180	43.47
	Present	1,2			0.0905	150.71
3.0	Ref. 14				0.0872	148.82
	Present	2,2			0.4026	103.68
	Ref. 14				0.3742	101.23
	Present	3,2			0.1451	133.07
	Ref. 14				0.1045	118.02
	Present	4,2			0.1060	134.85
	Ref. 14				0.0833	119.16
	Present	1,3				
	Ref. 14					
	Present	2,3				
	Ref. 14					
	Present	3,3			0.3995	87.62
	Ref. 14				0.3936	87.63
	Present	4,3			0.2761	88.80
3.0	Ref. 14				0.2797	88.52
	Present	1,4				
	Ref. 14					
	Present	2,4				
	Ref. 14					
	Present	3,4	0.4774	0.00	0.5349	30.54
	Ref. 14		0.4683	0.00	0.5253	30.03
	Present	4,4	0.2902	0.00	0.4555	49.35
	Ref. 14		0.2944	0.00	0.4531	47.28

[a] Modes are defined in Table 2.

VII. Calculations

Calculations of unsteady aerodynamic loads for coplanar and nonplanar configurations with control surfaces for various reduced frequencies and Mach numbers have been performed in order 1) to demonstrate the applicability of the present method by comparison with available calculated and experimental data, and 2) to contribute to the AGARD data base for interfering lifting surfaces,[9] especially for those configurations where the results of other references are in disagreement or scarce.

All configurations are symmetric with respect to the x-z plane and also the displacement modes are symmetric or antisymmetric. Therefore only one-half of the configuration need be considered when the contribution of the other half is properly accounted for. The generalized aerodynamic coefficients were obtained by integrating over *one*-half of the configuration. The reference length in all calculations is 1.

Isolated Wings

Rectangular Wing

In Fig. 3 the pressure distributions in the midsection of a rectangular wing performing a pitching motion about the midchord are compared. They have been obtained with the present two- and three-dimensional method. An excellent agreement is shown. The spanwise load distribution for the same wing and displacement mode are compared in Fig. 4 with Laschka's results.[10] Again a good agreement is shown.

AGARD Swept Wing with Control Surface

The generalized aerodynamic coefficients for the AGARD swept wing with control surface (Fig. 5) are compared in Table 1 with the results of Refs. 1, 11, and 12 for the

Table 4 AGARD tail-fin interference, z tail = 1.2.
Modes[a]: 1) fin bending; 2) fin twisting; 3) tail rolling

Mach no.	Methods (No. elements)	Q_{mn}	$k=0.0$ MOD(Q)	$k=0.0$ ARG(Q), deg	$k=1.5$ MOD(Q)	$k=1.5$ ARG(Q), deg
	Present (105)				0.8186	89.35
	Ref. 1 (105)	1,1			0.7801	90.92
	Ref. 16[b]				7.1943	79.27
	Present				0.0887	128.57
1.6	Ref. 1	2,1			0.0905	131.93
	Ref. 16				0.2094	71.51
	Present				0.1053	−63.29
	Ref. 1	3,1			0.1898	72.84
	Ref. 16				2.5818	79.67
	Present		0.7948	0.00	0.7115	13.23
	Ref. 1	1,2	0.8089	0.00	0.6860	18.22
	Ref. 16		2.7068	0.00	1.5532	−24.23
	Present		0.0807	0.00	0.2600	63.36
	Ref. 1	2,2	0.0970	0.00	0.2671	67.30
	Ref. 16		0.3511	0.00	0.3924	43.99
	Present		0.1828	0.00	0.0470	−166.97
	Ref. 1	3,2	0.2258	0.00	0.1397	177.11
	Ref. 16		0.5621	0.00	0.3766	−68.31
	Present				0.0954	61.86
	Ref. 1	1,3			0.0873	64.92
	Ref. 16				2.4391	87.06
	Present				0.0316	48.18
1.6	Ref. 1	2,3			0.1812	7.90
	Ref. 16				0.0238	27.75
	Present				0.7177	88.47
	Ref. 1	3,3			0.6686	89.79
	Ref. 16				1.0056	88.01

[a] Modes are defined in Table 5. [b] The results of Ref. 16 were obtained with fin reflection.

Table 5 Displacement modes of AGARD tail-fin configuration

Tail	Fin	Mode
$h_1=0$	z^2	Fin bending
$h_2=0$	$z(x-0.875\,z-3.0)$	Fin twisting
$h_3=y$	0	Tail rolling

following modes:

1) heaving, $h_1=1$
2) pitching about the midchord, $h_2=x-c/2$
3) chordwise bending, $h_3=(x-c/2)^2$
4) flapping of control surface, h_4

The coefficients are in good agreement.

Fighter-Type Wing¶

The spanwise load distributions for a fighter-type wing in the case of a pitching motion about the root midchord are compared in Fig. 6 with experimental results.[13] The agreement is satisfactory. The differences are of the same order as what has been reported for subsonic cases in Ref. 13.

¶Reference length is the midchord.

Interacting Coplanar Wings**

AGARD Wing-Tail Configuration

Figure 7 shows results for the AGARD wing-tail configuration. The displacement modes of the configuration are defined in Table 2.

Figure 7 shows the comparison of the present results with those of Refs. 1, 14, and 15. The results of the present method and those of Ref. 14 are in good agreement. The other results agree only in tail-due-to-tail and wing-due-to-wing modes. Probably these methods have not taken into account the wake properly.

Interacting Nonplanar Wings**

AGARD Wing-Tail Configuration

Table 3 compares the present results for the AGARD wing-tail configuration, where the tail is located at $z=0.6$, with those of Ref. 14. The displacement modes are the same as for the planar wing-tail configuration.

For $k=0$ all generalized aerodynamic forces are in good agreement. For $k=1.5$ this is only true for wing-due-to-wing and tail-due-to-tail modes. The interference effects do not agree in magnitude. Also here, this disagreement is probably due to the contribution of the wake.

**In all interacting cases the present calculations were performed using the new formulation as well as according to the original method. The results did not show significant differences.

Table 6 AGARD wing-tail-fin interference, z tail = 0.0.
Modes[a]: 1) wing twisting; 2) tail pitching; 3) fin bending; 4) fin twisting

Mach No.	Methods (No. elements)	Q_{mn}	$k=0.0$ MOD(Q)	$k=0.0$ ARG(Q), deg	$k=1.5$ MOD(Q)	$k=1.5$ ARG(Q), deg
	Present (240)	1,1	0.0285	180.00	0.2512	68.57
	Ref. 1 (253)		0.0202	180.00	0.2601	71.18
	Present	2,1	0.1360	180.00	0.0618	83.21
	Ref. 1		0.1333	180.00	0.2803	129.40
	Present	3,1	0.1000	180.00	0.0495	8.36
	Ref. 1		0.0980	180.00	0.0502	11.38
	Present	4,1	0.0459	180.00	0.0293	30.16
	Ref. 1		0.0460	180.00	0.0367	49.14
3.0	Present	1,2				
	Ref. 1					
	Present	2,2	0.3366	0.00	0.4446	45.86
	Ref. 1		0.3420	0.00	0.4510	45.93
	Present	3,2	0.0183	180.00	0.0143	66.04
	Ref. 1		0.0176	180.00	0.0133	71.57
	Present	4,2	0.0422	180.00	0.0269	90.64
	Ref. 1		0.0414	180.00	0.0262	103.03
	Present	1,3				
	Ref. 1					
	Present	2,3			0.0045	−170.33
	Ref. 1				0.0047	−168.93
	Present	3,3			0.4413	95.20
	Ref. 1				0.4397	95.48
	Present	4,3			0.0587	111.49
	Ref. 1				0.0583	111.84
	Present	1,4				
3.0	Ref. 1					
	Present	2,4	0.0137	180.00	0.0086	95.35
	Ref. 1		0.0144	180.00	0.0090	100.87
	Present	3,4	0.3396	0.00	0.3535	18.87
	Ref. 1		0.3400	0.00	0.3514	19.45
	Present	4,4	0.0534	0.00	0.1196	61.86
	Ref. 1		0.0545	0.00	0.1200	62.68

[a] Modes are defined in Tables 2 and 5.

AGARD Tail-Fin Configuration

The generalized aerodynamic coefficients for a T-tail configuration with the tail mounted on the fin at $z=1.2$, are compared in Table 4 with results of Refs. 1 and 16 for the displacement modes shown in Table 5.

Except for $Q_{3,1}$, $Q_{3,2}$, and $Q_{2,3}$, a good agreement has been obtained between the present results and those of Ref. 1. No agreement has been found with the results of Ref. 16. The disagreement is possibly due to the way of determining the generalized aerodynamic coefficients. The present results have been obtained by taking into account half the force acting on the tail and the fin.

AGARD Wing-Tail-Fin Configuration

Table 6 compares the present results for the AGARD wing-tail-fin configuration, where the tail is located at $z=0$, with those of Ref. 1.

The displacement modes are 1) wing twisting, 2) tail pitching, 3) fin bending, 4) fin twisting, as defined in the previous cases. For $k=0$ the generalized aerodynamic coefficients are in excellent agreement. For $k=1.5$ there is a good agreement in all modes except for tail-due-to-wing and fin-due-to-wing modes.

VIII. Conclusions

A potential gradient method has been developed to determine loads on harmonically oscillating interfering nonplanar wings in supersonic flow along similar lines, as described in Ref. 1.

The original method of Ref. 1 has been improved by a more efficient computation of the integral over the wake and far field elements.

The applicability of the present method has been demonstrated by comparing calculated unsteady airloads and generalized aerodynamic coefficients with results of the

original method and also of other methods. A satisfactory agreement has been found with experimental data available for a fighter-type wing.

Complete agreement has not been obtained in certain interacting unsteady ($k \neq 0$) cases, which is attributed to a more accurate computation of the wake contribution in the present method.

Acknowledgment

This investigation was carried out under contract for the Scientific Research Division of the Directorate of Materiel, Royal Netherlands Air Force (RNLAF).

References

[1] Jones, W.P. and Appa, K., "Unsteady Supersonic Aerodynamic Theory for Interfering Surfaces by the Method of Potential Gradient," NASA CR-2898, 1977.

[2] Miles, J.W., "The Potential Theory of Unsteady Supersonic Flow," Cambridge University Press, Cambridge, England, 1959.

[3] Jones, W.P., "Supersonic Theory for Oscillating Wings of any Planform," R&M 2655, June 1948.

[4] AGARD, *Manual on Aeroelasticity,* Vol. VI, 1964.

[5] Harder, R.L. and Rodden, W.P., "Kernel Function for Non-Planar Oscillating Surfaces in Supersonic Flow," *Journal of Aircraft,* Vol. 8, Aug. 1971, pp. 667-679.

[6] Cunningham, A.M. Jr., "The Application of General Aerodynamic Lifting Surface Elements in Unsteady Transonic Flow," NASA CR-112264, 1973.

[7] Rodden, W.P., Giesing, J.P., and Kalman, T.P., "New Developments and Applications of the Subsonic Doublet Lattice Method for Nonplanar Configurations," AGARD CP-80-71, Part 2, No. 4, 1971.

[8] Jordan, P.F., "Numerical Evaluation of the Three-Dimensional Harmonic Kernel," *Zeitschrift fuer Flugwissenschaften,* Vol. 24, No. 4, 1976, pp. 205-209.

[9] Rodden, W.P., "A Comparison of Methods Used in Interfering Lifting Surface Theory," *Manual on Aeroelasticity,* supplement, Vol. VI, AGARD-R-643, 1976.

[10] Laschka, B., "Der harmonisch schwingende Rechteckflügel bei Ueberschallströmung," Bericht der Ernst Heinkel Flugzugbau GmbH, 1960.

[11] Stark, V.J.E., "Calculation of Aerodynamic Forces on Two Oscillating Finite Wings at Low Supersonic Mach Numbers," SAAB TN 53, 1964.

[12] Fenain, M. and Guiraud-Vallee, D., "Numerical Calculations of Wings in Steady or Unsteady Supersonic Flow, Part 1: Steady Flow: Part 2: Unsteady Flow," *Recherches Aerospatiale,* No. 115, 1966-67.

[13] Tijdeman, H. et al., "Transonic Wind-Tunnel Tests on an Oscillating Wing with External Store," Part II: The Clean Wing, NLR TR 78106 U.

[14] Pollock, S.J. and Huttsell, L.J., "Applications of Three Unsteady Aerodynamic Load Prediction Methods," AFFDL TR-73-147, May 1974.

[15] Tsen, K. and Morino, L., "A New Unified Approach for Analyzing Wing-Body-Tail Configurations with Control Surfaces," AIAA Paper 76-418, July 1976.

[16] Mykytow, W.J., Olsen, J.J., and Pollock, S.J., "Application of AFFDL Unsteady Load Prediction Methods to Interfering Surfaces," Paper No. 7 presented at the AGARD Symposium on Unsteady Aerodynamics for Aeroelastic Analyses of Interfering Surfaces, Tønsberg, Norway, AGARD CP-80-71, 1970.